PRODUCTION OF CHARMONIUM AND JETS
IN ULTRARELATIVISTIC PROTON–PROTON COLLISIONS

A.V. Dieiev*, V.V. Kotlyar**, N.I. Maslov**

* V.N. Karazin Kharkov National University
Svoboda Sq. 4, Kharkov 61022, Ukraine
** National Science Center «Kharkov Institute of Physics and Technology»
Akademichna 1, 61108 Kharkov, Ukraine
E-mail: kotlyarv@kipt.kharkov.ua

Production of J/ψ–meson in association with jet in proton–proton collisions is studied at energy $s^{1/2} = 8$ TeV. Jet pair production at $s^{1/2} = 7$ TeV is considered briefly. Event generator Pythia 8 is employed in the simulations of the reactions. Distributions that depend on differences of transverse momenta, rapidities y_{mj}, and azimuthal angles φ_{mj} of the meson and jet are calculated. It is analyzed, how gluon radiation in initial and final states of the partonic processes along with multiple parton interactions influence the observables. Shapes of $(y_{mj}, \varphi_{mj}, y_{J/\psi})$– and $(y_{mj}, p_{T\,J/\psi}, y_{J/\psi})$–distributions, with $p_{T\,J/\psi}$ ($y_{J/\psi}$) being momentum (rapidity) of J/ψ, are shown to differ substantially for the mesons, emitted in the central and forward regions. The observables, measurements of which will help to impose severe constraints on used models, are discussed.
KEY WORDS: event generator Pythia, charmonium, jet production, proton–proton collisions, the LHC, experiments ALICE, ATLAS, CMS, LHCb

РОЖДЕНИЕ ЧАРМОНИЯ И СТРУЙ В СТОЛКНОВЕНИЯХ УЛЬТРАРЕЛЯТИВИСТСКИХ ПРОТОНОВ
А.В. Деев*, В.В. Котляр**, Н.И. Маслов**

* Харьковский национальный университет им. В.Н. Каразина
пл. Свободы, 4, г. Харьков, 61022, Украина
** Национальный Научный Центр «Харьковский Физико-Технический Институт»
ул. Академическая 1, г. Харьков, 61108, Украина

Рождение J/ψ мезона совместно со струёй в протон–протонных соударениях изучается при энергии $s^{1/2} = 8$ ТэВ. Кратко рассматривается рождение пар струй при $s^{1/2} = 7$ ТэВ. При моделировании реакций используется генератор событий Пифия 8. Рассчитаны распределения, которые зависят от разностей поперечных импульсов, быстрот y_{mj} и азимутальных углов φ_{mj} мезона и струи. Анализируется влияние на наблюдаемые излучения глюонов в начальном и конечных состояниях партонных процессов, а также многократного рассеяния партонов. Демонстрируется, что форма $(y_{mj}, \varphi_{mj}, y_{J/\psi})$– и $(y_{mj}, p_{T\,J/\psi}, y_{J/\psi})$–распределений, где $p_{T\,J/\psi}$ ($y_{J/\psi}$) есть поперечный импульс (быстрота) J/ψ, существенно различается для мезонов, рождающихся в центральной области и под малыми углами к оси пучков. Исследуются наблюдаемые, измерение которых может быть полезным для получения строгих ограничений на используемые модели.
КЛЮЧЕВЫЕ СЛОВА: генератор событий Пифия, чармоний, рождение струй, протон–протонные столкновения, Большой адронный коллайдер ЦЕРН, эксперименты ALICE, ATLAS, CMS, LHCb

НАРОДЖЕННЯ ЧАРМОНІЯ ТА СТРУМЕНІВ У ЗІТКНЕННЯХ УЛЬТРАРЕЛЯТИВІСТСЬКИХ ПРОТОНІВ
А.В. Дєєв*, В.В. Котляр**, М.І. Маслов**

*Харківський національний університет ім. В.Н. Каразіна
пл. Свободи 4, 61022, м. Харків, Україна
** Національний Науковий Центр «Харківський Фізико-Технічний Інститут»
вул. Академічна 1, м. Харків, 61108, Україна

Народження J/ψ мезону разом із струменем в протон–протонних зіткненнях вивчається при енергії $s^{1/2} = 8$ ТеВ. Стисло розглядається народження пар струменів при $s^{1/2} = 7$ ТеВ. При моделюванні реакцій використовується генератор подій Піфія 8. Розраховуються розподіли, що залежать від різниць поперечних імпульсів, бистрот y_{mj} та азимутальних кутів φ_{mj} мезона та струменю. Аналізується вплив на спостережувані випромінювання глюонів в початковому та кінцевому станах партонних процесів, а також багаторазового розсіяння партонів. Демонструється, що форма $(y_{mj}, \varphi_{mj}, y_{J/\psi})$– та $(y_{mj}, p_{T\,J/\psi}, y_{J/\psi})$–розподілів, де $p_{T\,J/\psi}$ ($y_{J/\psi}$) є поперечний імпульс (бистрота) J/ψ, істотно відрізняються для мезонів, що народжуються в центральній області та під малими кутами відносно осі пучків. Досліджуються спостережувані, вимірювання яких може бути корисним для отримання строгих обмежень на моделі, що використовуються.
КЛЮЧОВІ СЛОВА: генератор подій Піфія, чармоній, народження струменів, протон-протонні зіткнення, експерименти ALICE, ATLAS, CMS, LHCb, великий коллайдер адронів ЦЕРН

In recent years, production of charmonia, including $J/\psi(1S)$–meson,

$$p + p \to J/\psi(1S) + X, \tag{1}$$

and of jets

$$p + p \to jet + X \tag{2}$$

is receiving much attention in experiments at the LHC.

49

physical series «**Nuclei, Particles, Fields**», issue **1** /57/   Production of charmonium...

Production of prompt J/ψ has been studied by ALICE [1], ATLAS [2], CMS [3,4], and LHCb [5] collaborations. ALICE has obtained the data for the differential cross section in the central region $|y_{J/\psi}| < 0.9$ and $1.3 \text{GeV/c} < \; < p_{TJ/\psi} < 10 \text{GeV/c}$, where $y_{J/\psi}(p_{TJ/\psi})$ is J/ψ rapidity (transverse momentum). ATLAS has carried out measurements for four rapidity bins covering $|y_{J/\psi}| < 2.4$ from $p_{TJ/\psi} = 1 \text{GeV/c}$ in $2 < |y_{J/\psi}| < 2.4$ and $p_{TJ/\psi}$ up to 70 GeV/c in $0.75 < |y_{J/\psi}| < 1.5$. CMS data are in five rapidity bins with $|y_{J/\psi}| < 2.4$ for $p_{TJ/\psi}$ up to 70 GeV/c in central region $|y_{J/\psi}| < 0.9$, and up to 30 GeV/c for $2.1 < |y_{J/\psi}| < 2.4$. Detailed measurements [5] in the forward region have been performed by LHCb for five rapidity slices 2, 2.5,... 4, 4.5 and $p_{TJ/\psi}$ up to 14 GeV/c...11 GeV/c.

Discussion of models, used in the calculations of the cross sections for (1), and of interpretation of the data can be found, e.g. in [6–8], and in the papers cited therein. Thus, it was shown in [8] that the computed cross sections depend noticeably on the renormalization and factorization scales. The variations due to these uncertainties in the calculations are substantial for $p_{TJ/\psi} < 10 \, GeV/c$, i.e. in the region of intensive experimental activity.

Jet production has been also studied in detail at the LHC. Here we mention results [9] of LHCb collaboration on jet pair production in the forward region, that are discussed below.

The obtained data for J/ψ and jet production allow to test theoretical predictions, based on perturbative QCD, computations of processes beyond the leading order, models that intend to treat non-perturbative effects and to describe fragmentation of partons.

The aim of this paper is to calculate observables in production of J/ψ in association with jet

$$p + p \to J/\psi(1S) + jet + X, \tag{3}$$

and of jet pairs $p + p \to jet_1 + jet_2 + X$ under conditions of the experiments at the LHC and to analyze mechanisms of the reactions in various kinematic regions.

FRAMEWORK FOR SIMULATION OF CHARMONIUM AND JET PRODUCTION

The present analysis of (2) and (3) is performed with the help of event generator Pythia 8.170 [10,11]. Within the used approach charmonia originate from $c\bar{c}$ – pairs, created in collisions of incoming partons. Color–singlet (a = 1) and color–octet (a = 8) intermediate $c\bar{c}$ – states that are included in the calculations are listed in Table 1. Orbital angular momentum, total spin, and total angular momentum are denoted by *L, S*, and *J*. For brevity these processes are referred below as "charmonium" group.

Prompt J/ψ–mesons are produced directly in gluon–gluon scattering

$$g + g \to J/\psi(1S) + g \tag{4}$$

or in decays of color–singlet and color–octet $c\bar{c}$ –states, e.g. in $\chi_{cJ} \to \gamma + J/\psi$ and in $c\bar{c}\,[^{2S+1}L_J(8)] \to g + J/\psi$.

Integral cross sections of the partonic processes, obtained with Pythia 8 at total energy $\sqrt{s} = 8$ TeV, are displayed in Fig. 1.

Set of parameters "4C" [11,12], parton distribution functions CTEQ6L1 [13] are used throughout this work. The minimum

Table 1.

Partonic processes and quantum numbers
of intermediate $c\bar{c}$ – states

process	$^{2S+1}L_J(a)$	
	a=1	a=8
$gg \to c\bar{c}\,[^{2S+1}L_J(a)]\,g$	$^3S_1$ and ^3P_J with $J = 0,1,2$	$^3S_1$, $^1S_0$, $^3P_0$
$qg \to c\bar{c}\,[^{2S+1}L_J(a)]\,q$	^3P_J with $J = 0,1,2$	
$q\bar{q} \to c\bar{c}\,[^{2S+1}L_J(a)]\,g$,		

value of transverse momentum is chosen to be $p_{Tmin} = 10$ GeV/c. Values $c_R = c_F = 1$ are accepted for scale parameters that determine renormalization and factorization scales.

The processes with integral cross section $\sigma_{int}(c\bar{c}, \tau, p_T) > 50$ nb are included in Fig. 1. In addition, cross section for (4) is shown for comparison. Contribution of this process turns out to be not essential in the current studies. Index τ labels partonic processes. The processes in Fig. 1 give more that 90% of cross section $\sigma_{int}(c\bar{c}, p_T) = \sum_{\tau = 1,...,19} \sigma_{int}(c\bar{c}, \tau, p_T)$, that is a sum for all contributions in correspondence with Table 1. Integral cross section for J/ψ production $\sigma_{int}(J/\psi, p_T) = 840 \, nb$ is visibly lower than $\sigma_{int}(c\bar{c}, p_T) = 1.314 \, \mu b$, as far as the $c\bar{c}$ – states not always evolve into the meson.

J/ψ–mesons also come from decay of b–hadrons, especially from B–mesons. Such non–prompt J/ψ are disentangled from prompt ones in experiments [1-5] at the LHC. Essential mechanism of B–meson production, incorporated in Pythia, is string fragmentation. Since correlations of prompt J/ψ with jet in (3), where jet is generated by a parton in final states of "charmonium" processes, are intended to be studied below, the non–prompt J/ψ are not discussed in detail.
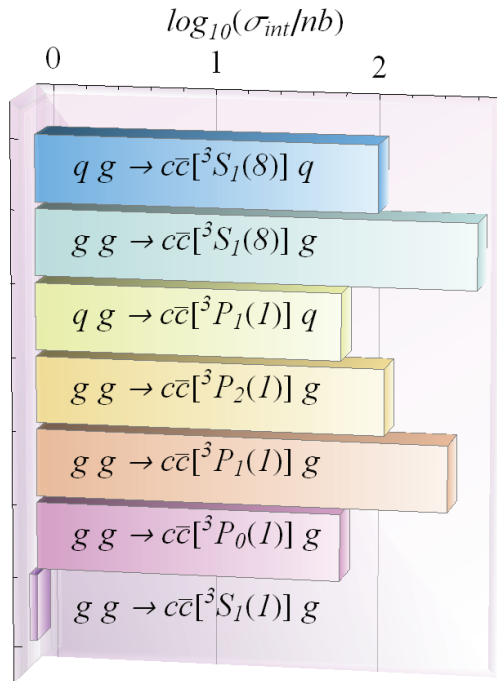
$log_{10}(\sigma_{int}/nb)$

Fig. 1. Integral cross sections of some partonic processes, those result in creation of J/ψ meson.
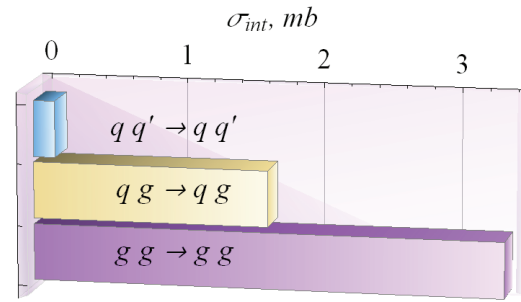
σ_{int}, mb

Fig. 2. Integral cross sections of some QCD processes, with that jet production is simulated.

As seen from Fig. 1, processes with two gluons in the initial states bring dominant contributions to $\sigma_{int}(c\bar{c}, p_T)$. The same holds for "hard QCD" processes [10,11], used in analysis of jet production (2). Some of them, which have the integral cross sections $\sigma_{int}(QCD, \tau, p_T) > 100$ μb, are shown in Fig. 2. These processes give more than 98% of the cross section $\sigma_{int}(QCD, p_T) = 5.36$ mb, where $\sigma_{int}(QCD, p_T)$ involves all included "hard QCD" processes. Relatively large values of the cross sections for processes due to gluon scattering may provide for enhanced sensitivity of the observables to gluon distribution functions.

To find jets the generated events are analyzed with SlowJet program, being a component of Pythia 8. In searches of jets the anti-k$_T$ algorithm is employed. The clusters with total transverse momenta, that do not exceed 10 GeV/c, are not considered as jets. The *r*–parameter, that determine jet–cone radius in rapidity–azimuthal angle space, is 0.7. Pseudorapidity region *η*>6 is excluded from jet searches. This pseudorapidity region corresponds to the polar angles $0 < \theta < 0.284°$. For a particle with energy *E* and 3–momentum $\vec{p} = (p_x, p_y, p_z)$ rapidity *y* and pseudorapidity *η* are defined as

$$y = \frac{1}{2} \ln \frac{E + p_z}{E - p_z}, \quad \text{and} \quad \eta = \frac{1}{2} \ln \frac{|\vec{p}| + p_z}{|\vec{p}| - p_z}.$$

The pseudorapidity and polar angle *θ* are related by $\eta = -\ln \tan(\theta / 2)$.

Neutrinos and particles, that participate neither in strong nor in electromagnetic interactions, are left out.

MULTIPARTON INTERACTIONS, INITIAL–, AND FINAL–STATE RADIATION IN PRODUCTION OF J/ ψ–MESONS AND JETS

In this section we discuss influence of multiparton interactions (MPI), initial–state radiation (ISR), and final–state radiation (FSR) on observables in production of prompt J/ψ and jets. Throughout the paper simulation of proton–proton collisions is carried out under conditions of the LHC experiments at total energy $\sqrt{s} = 7$ TeV and 8 TeV.

As shown in Fig. 3, multiplicities of charged particles, obtained with "charmonium" and with "hard QCD" processes, change qualitatively when MPI, ISR, and FSR are switched on. Inclusion of these mechanisms results in substantial increase of event number in region $n_{ch} \geq 50$. In calculations with MPI, ISR, and FSR functions $1/N_{total} N(n_{ch})$ for "charmonium" and "hard QCD" groups of partonic processes do not differ more than about 10% for $n_{ch} \approx 30...170$. Total number of generated events is denoted by N_{total}.

With inclusion of MPI, ISR, and FSR, jet multiplicities in (2) and (3) vary largely than charged particle multiplicities in (1) and (2), as it can be inferred from comparison of dash–dotted and solid curves in Figs. 4 and in Figs. 3. In simulations with "charmonium" (with "hard QCD") processes, when MPI, ISR, and FSR are not included, one (two) jet(s) are mainly produced in (3) (reaction (2)). Two (three) or more jets can be created in these reactions, when MPI, ISR, and FSR are taken into account. In Fig. 4 the multiplicities for (2) and (3), computed without ISR, FSR, and MPI, are multiplied by 0.6 and 0.5. For (2) $N_{events} = N_{total}$, while for (3) N_{events} is number of events, in which J/ψ is found.

Figs. 5 and 6 demonstrate that MPI, ISR, and FSR visibly manifest themselves in spectra for J/ψ in (1) and jets in (2) and (3). Reduction of the spectra of J/ψ in (1) and jets in (2) due to these mechanisms increases with J/ψ and jet transverse momenta $p_{T J/\psi}$ and $p_{T jet}$. Ratio of the distribution $dN / dp_{T J/\psi}$ ($dN / dp_{T jet}$), obtained without and with MPI,

51

physical series «**Nuclei, Particles, Fields**», issue **1** /57/   Production of charmonium...

ISR, and FSR, reaches ~6.3 (~7.1) at transverse momenta equal 100 GeV/c. At the same time, production of jets in (3) is enhanced by these mechanisms, as seen from Fig. 6. The corresponding ratio of the spectrum values is ~3.8 at $p_{T\,jet}$ = 100 GeV/c. In region of the transverse momentum $p_T \approx 40...100$ GeV/c, where distribution $dN/dp_{T\,jet}$ decreases more that in two orders of magnitude, ratio of jet spectra in (2) and (3), computed with MPI, ISR, and FSR, does not deviate considerably from 2, varying from ~1.9 up to ~2.2.
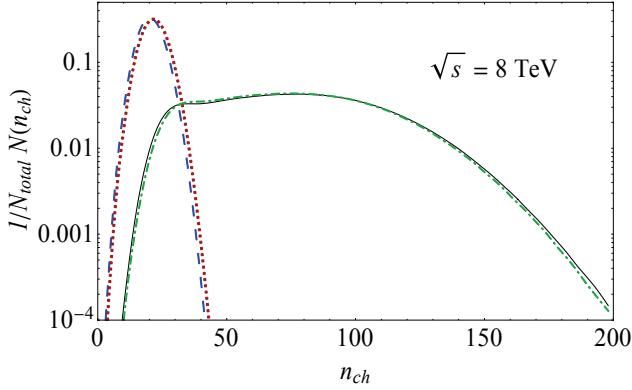
Fig. 3. Charge particle multiplicity for (1) (dashed and solid curves) and (2) (dotted and dash–dotted curves). Dashed and dotted (solid and dash–dotted) curves are obtained without (with) ISR, FSR, and MPI.
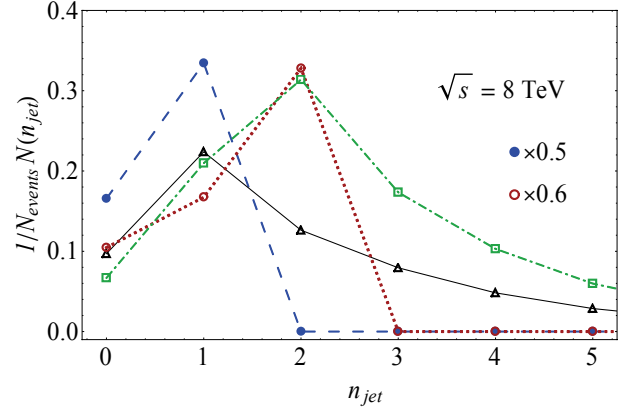
Fig. 4. Jet multiplicities in (2) and (3). Dotted and dash–dotted curves (○ and □) correspond to (2), dashed and solid curves (● and △) – to (3). Calculations without (with) ISR, FSR, and MPI are shown by dotted and dashed (dash–dotted and solid) curves.
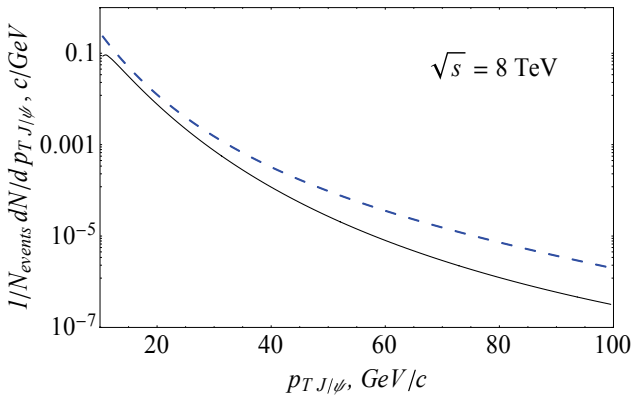

Fig. 5. Transverse momentum spectra of J/ψ in (1). Notation of the curves as in Fig 3.
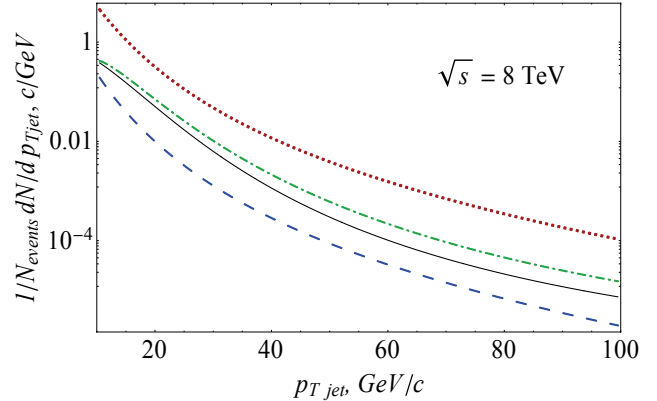
Fig. 6. Transverse momentum spectra of jets in (2) and (3). The curves are computed as in Fig 4.

To research into formation the transverse momentum spectra as well as distributions over $y_{mj} = y_{J/\psi} - y_{jet}$ and $\varphi_{mj} = \varphi_{J/\psi} - \varphi_{jet}$, where $y_{J/\psi}\,(\varphi_{J/\psi})$ and $y_{jet}\,(\varphi_{jet})$ are rapidities (azimuthal angles) of J/ψ and jet, we consider

$$dN(\xi,n)/d\xi = 1/\Delta y_n \int_{y_{n-1}}^{y_n} dy_{J/\psi}\, d^2 N(\xi, y_{J/\psi})/d\xi dy_{J/\psi} \tag{5}$$

with $\xi = p_{T\,mj}$, y_{mj} or φ_{mj}. The difference of J/ψ and jet momenta is $p_{T\,mj} = p_{T\,J/\psi} - p_{T\,jet}$. Rapidity bins are nume-rated by n, $\Delta y_n = y_n - y_{n-1}$ is width of the bin. In Figs. 7, 8, and in 13,…16 below, curves with label n=1,3,4,…6 are obtained with y_n=n. Rapidity of J/ψ takes on values $y_{J/\psi} \in (n-1, n)$ in n*th* bin. Curves for $1 < y_{J/\psi} < 2$ lie in between ones with n=1, 3, which are not well separated. Therefore, curves with n=2 are not displayed. Polar angle $\theta_{J/\psi}$ of the meson, emitted with rapidity $y_{J/\psi}$ = 0,1,2,3,…,7 and transverse momentum $p_{TJ/\psi}$ = 10 GeV/c, is 90°, 39°, 15°, 5.5°, 2.0°, 0.74°, 0.27°, 0.10°, respectively. With increase of $p_{TJ/\psi}$ up to 100 GeV/c angle $\theta_{J/\psi}$ grows less than in 5%.

Jet spectra $dN(p_{Tmj})/dp_{Tmj}$ have maxima near p_{Tmj}= 0 in simulations of (3) with MPI, ISR, and FSR switched off. As demonstrated in Fig. 7, peaks in distributions slightly shift into negative area of p_{Tmj} with increase of J/ψ rapidity $y_{J/\psi}$. Fig. 8 shows that inclusion of these mechanisms enhances the shifting and leads to broadening of the peaks. However, one can conclude from the Figs. that J/ψ–mesons and jets are produced in (3) with the transverse momenta that are close to each other.

Figs. 9 and 10 indicate that the rapidity distributions $dN(y_{J/\psi})/dy_{J/\psi}$ of J/ψ in (1) and $dN(y_{jet})/dy_{jet}$ of jets in (2) and (3) rapidly decrease with growth of $y_{J/\psi}$ and y_{jet}, when $y_{J/\psi}$, $y_{jet} > 3...4$. Rapidity distributions in (1) and (3),

shown by the dashed and solid curves, turn out to be almost insensitive to MPI, ISR, and FSR as opposed to ones in (2) and transverse momentum spectra in Figs. 5 and 6. Really, the distribution of J/ψ, created in (1), as functions of $y_{J/\psi}$, contains contributions of $p_{TJ/\psi}$ from a region adjacent to p_{Tmin}, since $dN(p_{TJ/\psi})/dp_{TJ/\psi}$ is a rapidly decreasing function. In this region the transverse–momentum spectrum is not affected strongly by the discussed mechanisms, as seen in Fig. 5. Transverse momenta of the jets and of the mesons in (3) do not duffer significantly, as demonstrated in Fig. 8.
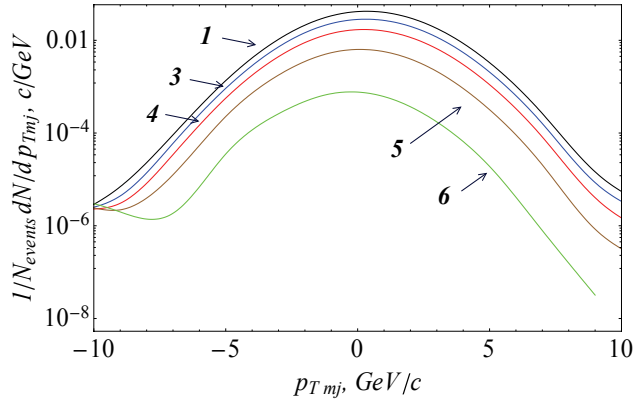

Fig. 7. Dependence of jet spectra $dN(p_{Tmj})/dp_{Tmj}$ in (3) on momentum p_{Tmj}.
Notation of the curves is explained in the text. Calculations are performed at $s^{1/2}$ = 8 TeV without ISR, FSR, and MPI.
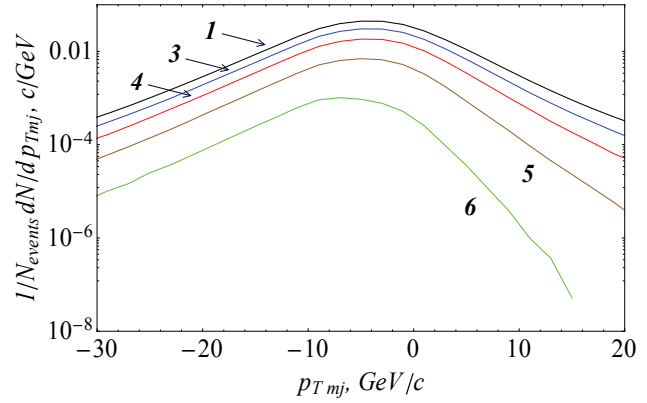
Fig. 8. The same as in Fig. 7.
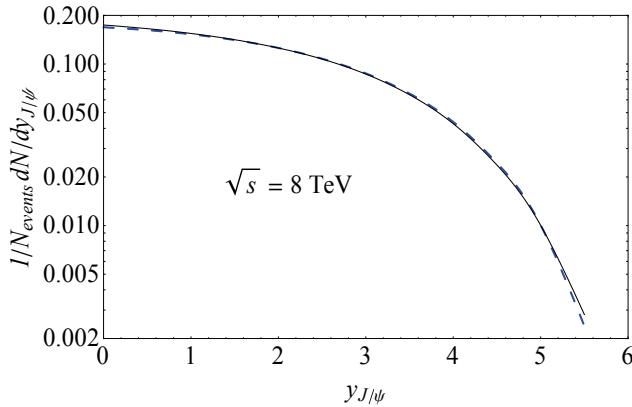The spectra are computed with inclusion of ISR, FSR, and MPI.

Fig. 9. Rapidity distributions of J/ψ in (1).
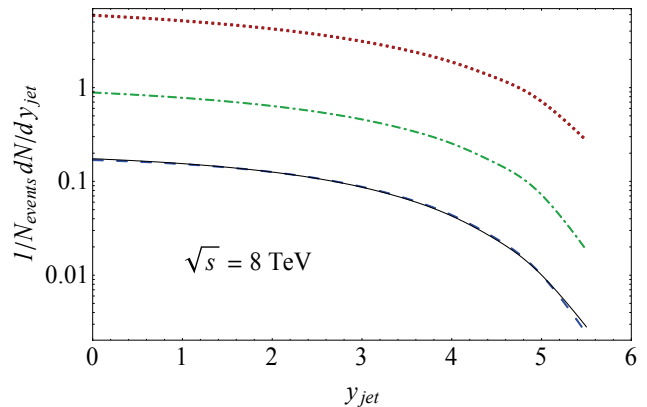Notation of the curves as in Fig 3.

Fig. 10. Rapidity distributions of jets in (2) and (3).
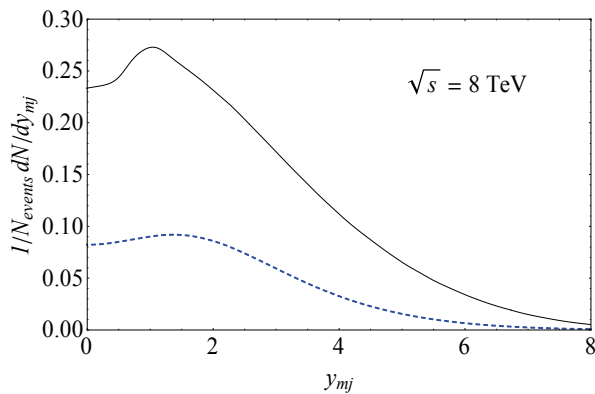Notation of the curves as in Fig 4.

Fig. 11. Distributions $dN(y_{mj})/dy_{mj}$ for (3).
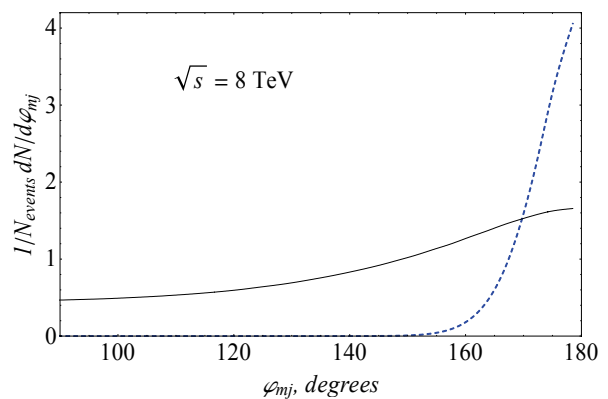Solid (dashed) curve is obtained with (without) ISR, FSR, and MPI.

Fig. 12. Distributions $dN(\varphi_{mj})/d\varphi_{mj}$ for (3).
Curves are computed as in Fig 11.

Next we consider how J/ψ and jets, emitted in (3), are separated in rapidity and azimuthal angle. With this aim the distributions $N(y_{mj})$ and $N(\varphi_{mj})$ that depend on y_{mj} and φ_{mj} are calculated. The distributions $N(y_{mj})$ satisfy $N(y_{mj}) = N(-y_{mj})$. According to Fig. 11 functions $N(y_{mj})$ have maxima at $y_{mj} \neq 0$. As displayed in Fig. 12, $N(\varphi_{mj})$

53

physical series «Nuclei, Particles, Fields», issue **1** /57/   Production of charmonium...

peaks at $\varphi_{mj} \sim 180°$. The transverse momentum vectors $\vec{p}_{TJ/\psi}$ and $\vec{p}_{Tjet}$ of J/ψ and jet, created in (3), are essentially oriented in opposite directions. Due to invariance with respect to rotations about the beam line and space inversion functions $N(\varphi_{mj})$ depend on $\vec{p}_{TJ/\psi} \cdot \vec{p}_{Tjet}$. The functions meet relations $N(\varphi_{mj}) = N(-\varphi_{mj})$, $N(\pi - \varphi_{mj}) = N(\pi + \varphi_{mj})$, etc. MPI, ISR, and FSR affect the distributions differently. Inclusion of these mechanisms results in $N(y_{mj})$ sharpening, but leads to broadening of $N(\varphi_{mj})$.

Character of y_{mj}–distributions depends on the rapidity $y_{J/\psi}$ of produced J/ψ–meson, as seen in Figs. 13 and 14. With increase of the meson rapidity $y_{J/\psi}$ distribution $dN(y_{mj}, y_{J/\psi})/dy_{mj}$ becomes broader and attains its maximum at larger values of y_{mj}. In the forward region, when $y_{J/\psi} \sim 5...6$, minimum at $y_{mj} \sim 0$ is most pronounced. Nevertheless, the cross sections in this region are about 10^2 times smaller than in central region for $y_{J/\psi} \sim 1...2$. Neither MPI, ISR, nor FSR alter significantly the shape of $N(y_{mj}, y_{J/\psi})$.
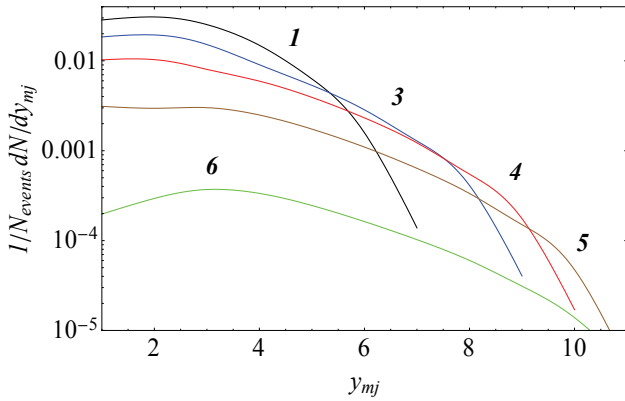

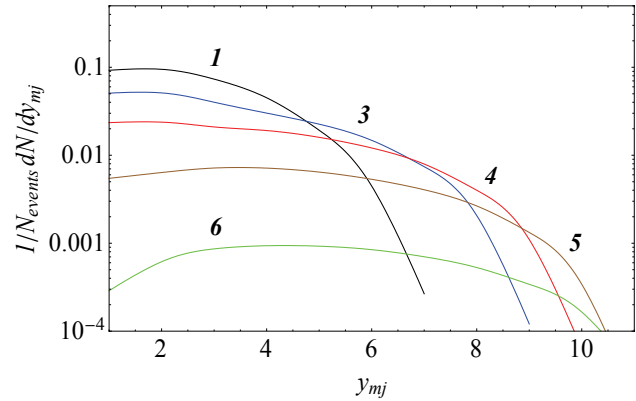Fig. 13. Distributions $dN(y_{mj}, n)/dy_{mj}$ for (3). Notation of the curves as in Fig 7.

Fig. 14. The same as in Fig. 13. Curves are computed as in Fig 8.

The shape of distribution $dN(\varphi_{mj}, y_{J/\psi})/d\varphi_{mj}$ is not recast in the considered interval of rapidity $y_{J/\psi}$, as illustrated by Figs. 15 and 16. Note, the distributions are symmetrical with respect to transformation $n\pi - \varphi_{mj} \to \varphi_{mj} - n\pi$, where n is an integer. Being calculated without MPI, ISR, and FSR, the distributions exhibit a ridge at $\varphi_{mj} \sim 180°$ and are localized at $\varphi_{mj} = 180° \pm 40°$. Within this approximation creation of more that one jet is strongly suppressed, as Fig. 4 shows, and single jet (if any) is ejected with the transverse momenta $\vec{p}_{Tjet}$, directed in opposite direction to momentum $\vec{p}_{TJ/\psi}$ of the meson. Such feature of the oversimplified picture in production of J/ψ–jet pairs does not survive in simulations with MPI, ISR, and FSR switched on. Fig. 16 demonstrates, that $dN(\varphi_{mj}, y_{J/\psi})/d\varphi_{mj}$ with $\varphi_{mj} = \pi \pm \varphi$ turns out to be a slowly decreasing function for $0 < \varphi < \pi/2$.
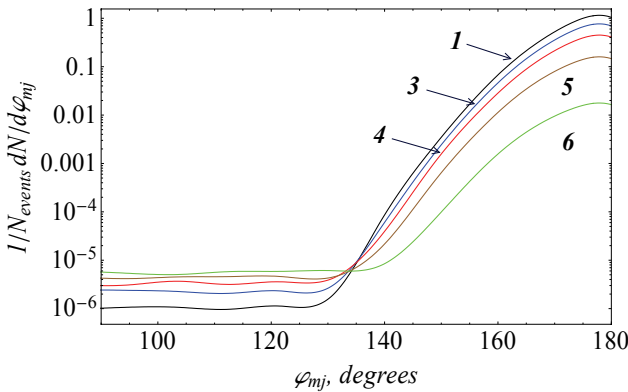

Fig. 15. Distributions $dN(\varphi_{mj}, y_{J/\psi})/d\varphi_{mj}$ for (3). Notation of the curves as in Fig 7.
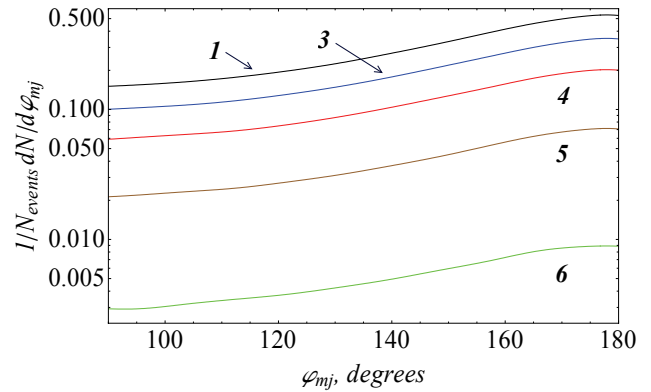
Fig. 16. The same as in Fig. 15. Curves are computed as in Fig 8.

Distance r for jet–pair production is about 2.5 both in (2) and (3), as one can see by comparing the dash–dotted and solid curves in Fig. 17. The quantity r is defined as $r = (\Delta y^2 + \Delta \varphi^2)^{1/2}$, where $\Delta y = y_i - y_k$, $\Delta \varphi = \varphi_i - \varphi_k$, with y_i and φ_i being the rapidity and the azimuthal angle of jet with number i. Since distances r between jets in J/ψ and jet

production take on close values, one can hope that the jet, created in association with the meson, can be disentangled from other jets. Dashed curve in Fig. 17 corresponds to very rare events, when more than one jet is produced in simulation of (3) without MPI, ISR, and FSR. Noticeable difference between solid and dashed curves stresses once more great significance of MPI, ISR, and FSR inclusion into calculations.

Our results for a spectrum in jet–pair production are compared with the recent LHCb data [9] in Fig. 18. In the LHCb experiment distribution of jet–pair invariant mass has been determined for jet pseudorapidities $2 \leq \eta_1, \eta_2 \leq 4.5$ and azimuthal angles $\| \varphi_1 - \varphi_2 \| - \pi \| < 0.7$. Transverse momenta of jets are restricted by $p_{T1}, p_{T2} \geq 20\,\text{GeV/c}$. From Fig. 18 one can conclude that both LHCb and our simulations with Pythia 6.4 and 8.170, performed with the parton distribution functions CTEQ6L, reproduce the invariant mass dependence of the measured spectrum.
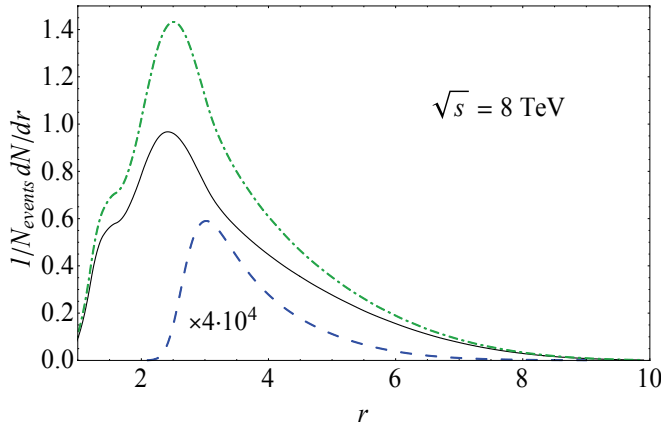

Fig. 17. Distance r between jets in (2) and (3). Curves are computed as in Fig 4.

Spectra in (2) and in $p + p \rightarrow jet_1 + jet_2 + X$ under conditions of the LHCb experiment are sensitive to the gluon density in a region of Bjorken x, characterized by the dashed and solid curves in Fig. 19. For comparison dash–dotted curve, obtained in simulations of (1), is displayed as well. Values of x, at which the distribution of x attains its maximum, are shown in this figure. The smaller x from two values of x for $2 \rightarrow 2$ partonic processes is selected.

At rapidity $y_{J/\psi} \sim 2,...2.5$ the spectra in (1) depend on gluon distribution at $x \sim 10^{-3.3}...10^{-3.5}$. In the same region of pseudorapidities η_{jet} spectra for the jet production are determined by gluon distribution at larger values of x. In the forward region observables in processes with jets are affected by gluon density at much smaller x.
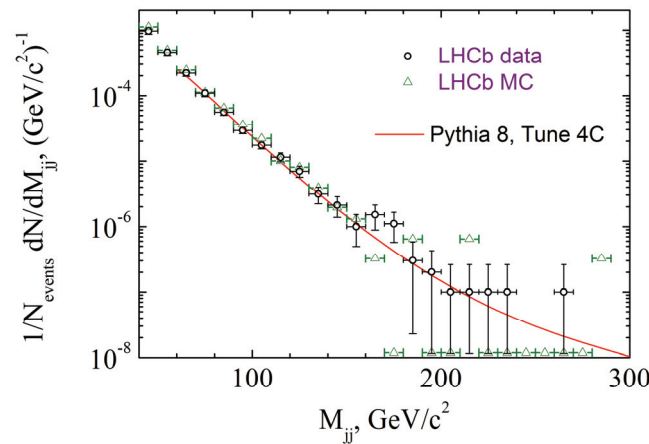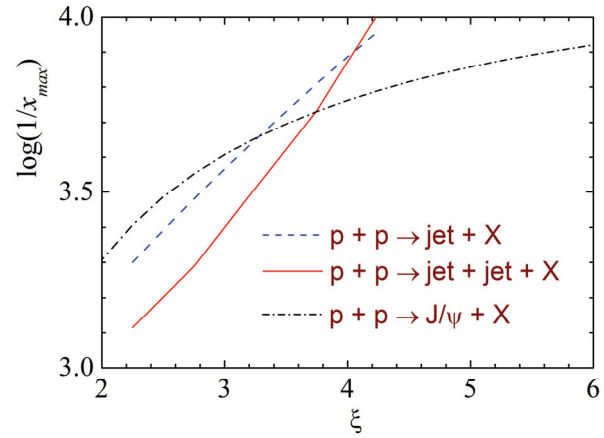

Fig. 18. Dijet spectrum as a function of dijet invariant mass. Circles (triangles) – results [9] of LHCb measurements (MC simulations) at $s^{1/2} = 7\,\text{GeV}$. The curve is computed in the present paper.

Fig. 19. Dependence of Bjorken $x_{Bj\,max}$ on values of ξ, where $\xi = \eta_{jet}$ or $y_{J/\psi}$ for jet or the meson production. Calculations are performed at $s^{1/2} = 7\,(8)\,\text{GeV}$ for jet (charmonium) production.

PROPERTIES OF SPECTRA IN J/Ψ AND JET PRODUCTION
IN SPECIFIC REGIONS OF THE PHASE SPACE

Above discussed distributions $N(p_{T J/\psi})$, $N(y_{mj})$, $N(\varphi_{mj})$, $N(y_{mj}, y_{J/\psi})$, and $N(\varphi_{mj}, y_{J/\psi})$ vary quantitatively with inclusion of MPI, ISR, and FSR, but keep qualitative features of their forms unchangeable. In this section we discuss how shapes of distributions

$$d^2 N(y_{mj}, \xi; n) / dy_{mj}\, d\xi = 1/\Delta y_n \int_{y_{n-1}}^{y_n} dy_{J/\psi}\, d^3 N(y_{mj}, \xi, y_{J/\psi}) / dy_{mj}\, d\xi\, dy_{J/\psi}, \qquad (6)$$

where $\xi = p_{T J/\psi}$ and φ_{mj}, are affected by these mechanisms.

Fig. 20 gives in detail the (y_{mj}, φ_{mj}) area of interest. Taking into account the symmetry properties of the distribution, the region, shown in the Fig., is reduced to $y_{mj} > 0$ and $\varphi_{mj} < \pi$. The curve with label n corresponds to φ_{mj} in bin $(\varphi_{n-1}, \varphi_n)$, where $\varphi_n = \pi n / 20$ with n being an integer. For $\varphi_{mj} < \varphi_6$ and $2\pi - \varphi_6 < \varphi_{mj} < 2\pi + \varphi_6$ the curves have a

55

physical series **«Nuclei, Particles, Fields»**, issue **1** /57/   Production of charmonium...

minima at $y_{mj} = 0$ and maxima at $y_{mj} \sim \pm(1.5...1.6)$. With increase of φ_{mj} in interval $\varphi_6 < \varphi_{mj} < 2\pi - \varphi_6$ the minima are filled and the functions gain a peak at $y_{mj} = 0$. Height of the peak goes up, when $\varphi_6 \leq \varphi_{mj} \leq \varphi_8$, then falls in $\varphi_8 \leq \varphi_{mj} < \varphi_{10}$, and growths again in $\varphi_{10} \leq \varphi_{mj} \leq \pi$. The same structure also manifests itself, but less distinctively, in distribution $d^2N(y_{mj}, \varphi_{mj})/dy_{mj}\,d\varphi_{mj} = \sum_n d^2N(y_{mj}, \varphi_{mj}; n)/dy_{mj}\,d\varphi_{mj}$, that collect contributions from all slices of J/ψ rapidity.
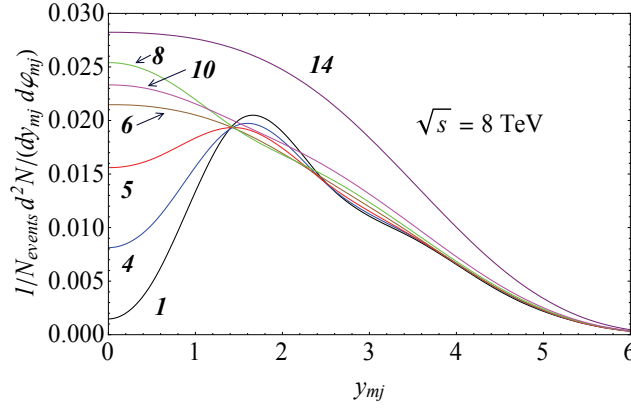

Fig. 20. Distribution $d^2N(y_{mj},\ \varphi_{mj},\ n)/(dy_{mj}d\varphi_{mj})$ for (3).
Labels on the curves are explained in the text.

Fig. 21 (a) and (b) show, that switching the mechanisms on fills in gap in vicinity of $y_{mj}\sim0$, $\varphi_{mj}\sim\pi$. These mechanisms smear the sharp peak, inherent to φ_{mj}–dependence in Fig. 21(a). The stretching is similar to that observed in Figs. 12, 15, and 16. Wings of the spreading peak acquire a structure visible in area of $|y_{mj}| \lesssim 5$, $|\varphi_{mj}|\lesssim2\pi/3$. The behavior of distribution (6) as a function of y_{mj} with $\xi = \varphi_{mj}$ and rapidity of the meson in central region $y_{J/\psi}\in(-1,1)$ substantially depends on values of φ_{mj}.
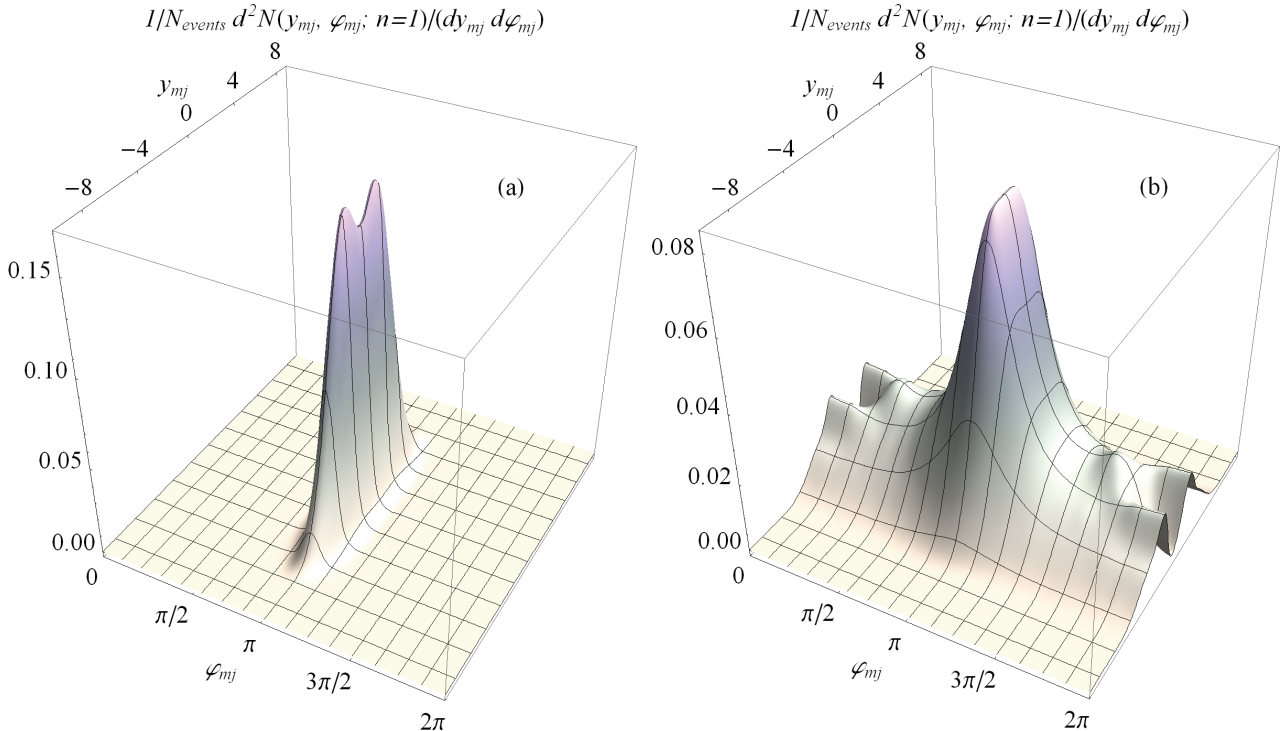

Fig. 21. Distribution $d^2N(y_{mj},\ \varphi_{mj},\ n)/(dy_{mj}d\varphi_{mj})$ for (3) with $y_{J/\psi}$ in interval (0,1) at $s^{1/2}$ = 8 GeV.
(a) – without MPI, ISR, and FSR, (b) – with inclusion of these processes.

As one can see from Fig. 21 (b) and Fig. 22 (a), (b), with growth of $y_{J/\psi}$ the distributions become wider in y_{mj}, peak at $y_{mj}\sim0$, $\varphi_{mj}\sim\pi$ splits and pronounced gap appears instead at the same place. The similar behavior is inherent to the distributions $dN(y_{mj};n)/dy_{mj}$, displayed in Fig. 14. Indistinct maxima at $\varphi_{max}\sim3\pi/8$ and $2\pi-\varphi_{max}$ in Fig. 21 (b) disappear in Fig. 22 (b).

$1/N_{events} \, d^2N(y_{mj}, \varphi_{mj}; n=5)/(dy_{mj} \, d\varphi_{mj})$

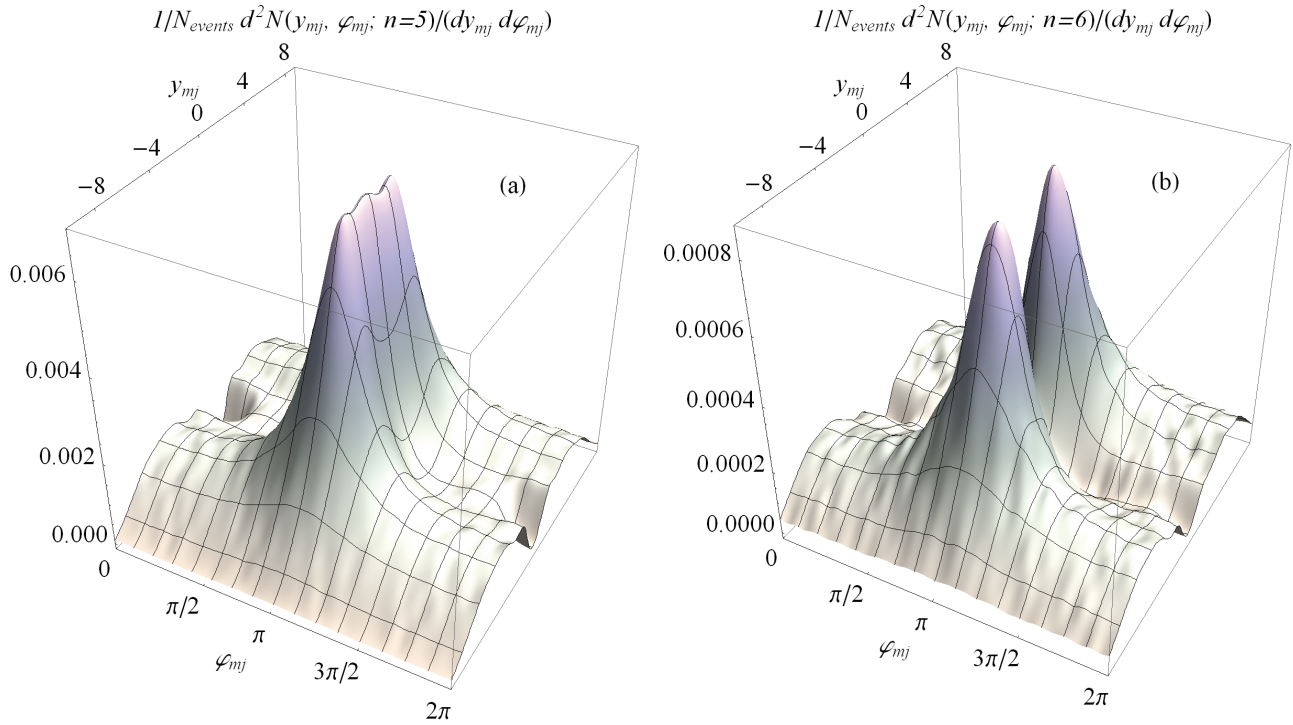$1/N_{events} \, d^2N(y_{mj}, \varphi_{mj}; n=6)/(dy_{mj} \, d\varphi_{mj})$

Fig. 22. The same as in Fig. 21 (b),
(a) – for $y_{J/\psi}$ in interval (4,5), (b) – (5,6).

The surface transformations with increase of the meson rapidity are followed by strong downfall of the distribution values that causes, inter alia, the short–range dithering outside of the peaks in Fig. 22. During simulation these areas receive smaller number of events, than regions in vicinity of maxima or in the central rapidity region.

In addition to scrutinizing the angular distributions, we examine properties of distributions (6) which depend on the transverse momentum $p_{TJ/\psi}$ of emitted J/ψ–meson. Transformations of the surface $N(y_{J/\psi}, y_{mj}, p_{TJ/\psi})$, when $y_{J/\psi}$ is running from the central into forward region, have much in common with those, observed in Figs. 20 and 21 for $N(y_{J/\psi}, y_{mj}, \varphi_{mj})$. The gap between two peaks in region $|y_{mj}| < 5$, $|p_{TJ/\psi}| < 5$ GeV/c deepens appreciably. The peaks, being partitioned to a small extent at $y_{J/\psi} \in (0,1)$, become well separated at $y_{J/\psi} \in (5,6)$.
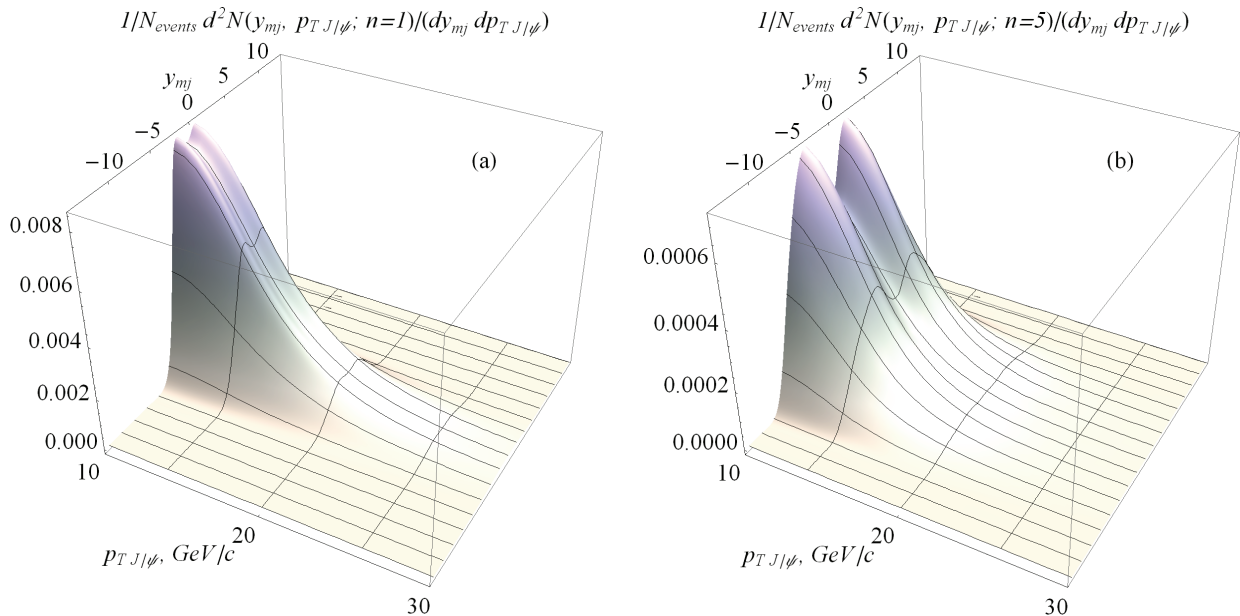
$1/N_{events} \, d^2N(y_{mj}, p_{T \, J/\psi}; n=1)/(dy_{mj} \, dp_{T \, J/\psi})$

$1/N_{events} \, d^2N(y_{mj}, p_{T \, J/\psi}; n=5)/(dy_{mj} \, dp_{T \, J/\psi})$

Fig. 23. Distribution $d^2N(y_{mj}, p_{TJ/\psi}, n)/(dy_{mj} d \, p_{TJ/\psi})$ for (3) at $s^{1/2} = 8$ GeV, computed with MPI, ISR, and FSR.
(a) – for $y_{J/\psi}$ in interval (0,1), (b) – (4,5).

From comparison of the distributions in Figs. 23 and 24 (a) one can see that the spectra, as a functions of $p_{TJ/\psi}$, fall down more steeply with rapidity growth. The splitting of peaks is hardly noticeable in the distributions summarized over the rapidity slices. Figs. 23 (b) and 24 (b) indicate that the observable is considerably influenced by MPI, ISR, and FSR, changing the form of the surface at $y_{J/\psi} \sim 0$ in the forward rapidity region.

57

physical series «**Nuclei, Particles, Fields**», issue **1** /57/   Production of charmonium...

$1/N_{events}\, d^2N(y_{mj},\, p_{T\,J/\psi};\, n=6)/(dy_{mj}\, dp_{T\,J/\psi})$ $1/N_{events}\, d^2N(y_{mj},\, p_{T\,J/\psi};\, n=5)/(dy_{mj}\, dp_{T\,J/\psi})$
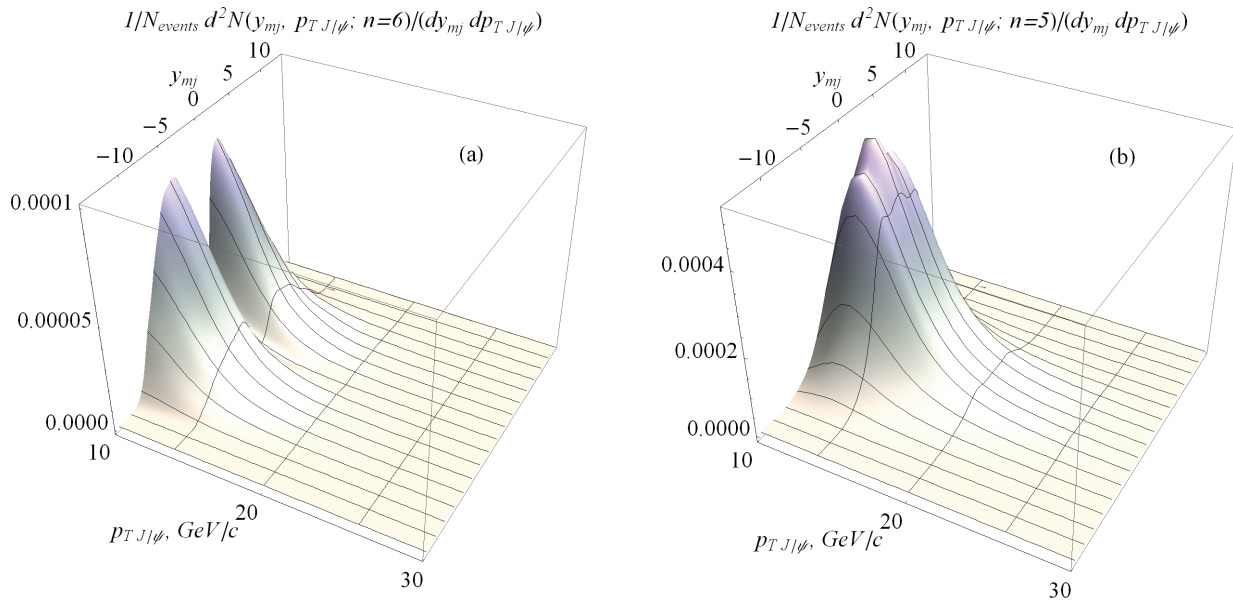
Fig. 24. The same as in Fig. 23,
(a) – with MPI, ISR, and FSR for $y_{J/\psi}$ in interval (5,6),
(b) – with these processes switched off for $y_{J/\psi}$ in interval (4,5).

CONCLUSIONS

Simulation of J/ψ production in proton–proton collisions is carried out with event generator Pythia 8.170. Events, in which the meson is created in association with at least one jet, are analyzed. The SlowJet program, included into Pythia 8 code, is employed for jet finding. Calculations are performed with set of parameter "4C" and parton distribution functions CTEQ6L1.

The observables, that are functions of J/ψ and jet transverse momenta, rapidities, and azimuthal angles, are calculated at $\sqrt{s} = 8$ TeV. Invariant mass spectrum in jet–pair production is computed at $\sqrt{s} = 7$ TeV. The results for the spectrum are in quite a good agreement with the LHCb data in the forward region.

It is shown that the observables in creation of J/ψ–jet pairs are strongly sensitive to initial– and final–state radiation of gluons, as well as to multiparton interactions. Qualitative features of these distributions are studied both in the central and forward regions of the meson emission. The distributions, those depend on differences of the J/ψ and jet rapidities y_{mj}, on differences of the azimuthal angles φ_{mj}, and on J/ψ rapidity $y_{J/\psi}$ or on y_{mj}, J/ψ transverse momentum $p_{T\,J/\psi}$, and $y_{J/\psi}$, i.e. being functions of $y_{mj}, \varphi_{mj}, y_{J/\psi}$, and $y_{mj}, p_{T\,J/\psi}, y_{J/\psi}$, vary substantially, when J/ψ rapidity passes from central into forward region. Surface shapes of the observables in the variables y_{mj}, φ_{mj} and $y_{mj}, p_{T\,J/\psi}$ undergo fairly large changes.

Measurements of the correlation observables in J/ψ–jet pair production prove to be within the potentialities of the detectors at the LHC. New data may serve as a sensitive testing ground for predictions, based on perturbative QCD, and for the approaches, which simulation of initial–, final–state radiation of gluons, and multiparton interactions is based on. The data allow one to infer the validity of models that aim to elucidate mechanisms of heavy–quark pair production and to place severe constraints on them.

REFERENCES

1. Abelev B. (ALICE Collaboration) Measurement of prompt J/ ψ and beauty hadron production production cross sections at mid-rapidity in pp collisions at beauty hadron production $\sqrt{s}$ = 7 TeV // JHEP. – 2012. – Vol.1211. – Iss.11. – 065. – 31 p.
2. Aad G. (ATLAS Collaboration) Measurement of the differential cross-sections of inclusive, prompt and non-prompt J/ ψ production in proton-proton collisions at $\sqrt{s}$ =7 TeV // Nucl. Phys. B. – 2011. – Vol. 850. – P. 387-444.
3. Khachatryan V. (CMS Collaboration) Prompt and non-prompt J/psi production in pp collisions at $\sqrt{s}$ = 7 TeV // Eur. Phys. J. C. – 2011. – Vol.71. – 1575. – 26 p.
4. Chatrchyan S. (CMS Collaboration) J/ψ and ψ(2S) production in pp collisions at $\sqrt{s}$ = 7 TeV // JHEP. – 2012. – Vol.1202. – Iss.2. – 011. – 46 p.
5. Aaij R. (LHCb Collaboration) Measurement of J/ ψ production in pp collisions at $\sqrt{s}$ =7 TeV // Eur. Phys. J. C. – 2011. – Vol.71. – 1645. – 17 p.
6. Brodzicka J., Corradi M., Schienbein I. et al. Heavy Flavour Working Group Summary // arXiv:1208.3379. – 2012. – 16 p.

7.   Bodwin G. Theory of Charmonium Production // arXiv:1208.5506. – 2012. – 25 p.
8.   Kotlyar V.V., Krupina N.V. J/ψ, Y, and B meson production in proton-proton collisions at the LHC // Prob. Atomic Sci. Technol. – 2012. – Vol.77, Iss.1 – P.183-187.
9.   Kucharczyk M. Jet measurements in LHCb and their relevance for PDF's // LHCb-TALK-2012-067. – 2012. – 15 p.
10.   Sjoestrand T., Mrenna S., Skands P. PYTHIA 6.4 Physics and Manual // JHEP. – 2006. – Vol. 0605. – 026. – 576 p.
11.   Sjoestrand T., Mrenna S., Skands P. A Brief Introduction to PYTHIA 8.1 // Comput. Phys. Commun. – 2008. – Vol.178.– P.852-867.
12.   Buckley A., Butterworth J., Gieseke S. et al. General-purpose event generators for LHC physics // Phys. Rept. – 2011. – Vol.504. – P.145-233.
13.   Pumplin J., Stump D.R., Huston J. et al. New generation of parton distributions with uncertainties from global QCD analysis // JHEP. – 2002. – Vol.0207. – Iss.7. – 012. – 44 p.

Dieiev Andrii V. is a student of Department of Physics and Technology at V.N. Karazin Kharkiv National University. He is involved in studies of silicon planar and microstrip detectors that are performed at "Physics of Radiation and Tracking Coordinate Detectors" Department at Institute of High–Energy Physics and Nuclear Physics in National Science Center Kharkov Institute of Physics and Technology.

Other area of his scientific interests belongs to phenomenology in high–energy physics. He participates in simulation of φ–, J/ψ–, Y–meson, Ξ–, Ω–baryon, and jet production in proton-proton scattering, investigation of reaction mechanisms, and analysis of correlation observables for the processes, in which pairs of φ, Ξ, Ω, jets, J/ψ–jet are created. Interpretation of results, obtained in the experiments at RHIC, Tevatron, and LHC, is essential direction of his work.